Journal of Flow Visualization & Image Processing, vol. 8, pp. 177-187, 2001

MOLECULAR TAGGING FLUORESCENCE VELOCIMETRY (MTFV) FOR LAGRANGIAN FLOW FIELD MAPPING INSIDE EVAPORATING MENISCUS: POTENTIAL USE FOR MICRO-SCALE APPLICATIONS

J. S. Park, H. J. Kim and K. D. Kihm[*]
Department of Mechanical Engineering, Texas A&M University, College Station, Texas 77843-3123, USA

The development of a molecular tagging fluorescence roelocimetry (MTFV) system is discussed and measurement results are presented for a meso-scale flow field of thermally driven capillary pore of 5 mm inner diameter that is tilted 5 ° from the horizon. The developed uses caged dextran conjugates of caged fluorescence dyes of less than 10 nm in size for tracers. The frequency-tripled ultraviolet (UV) band (λ= 355 nm) of a pulsed neodymium-yttrium-aluminum-garnet (Nd:YAG) laser uncages the molecules by photo-cleaving that is decomposition of a caging chemical group and a fluorescence chemical group. Then a continuous wave (CW) blue argon ion laser (λ=488 n) pumps the fluorescence of only those uncaged molecules, whose emission band is centered at λ= 518 nm, and a sequential recording of the fluorescence images are digitally recorded and analyzed for Lagrangian velocity field mapping. The use of the technique allows detailed measurements of the thermally driven three-dimensional flow inside a heated capillary pore. The measurement shows that the meniscus surface flow is mainly driven by the thermocapillary stress field, occurring due to the surface temperature gradient, while the bulk flow inside the pore is driven largely by the natural convection buoyancy.

INTRODUCTION

In attempting to use a regular particle image velocimetry (PIV) technique [1] for microscale flow field measurements, we encountered several problems: (1) the regular seeding particles that used for a light scattering effect are usually too large for most micro-scale applications; (2) when extremely fine seeding particles in the sub-micron range are used, the signal-to-noise ratio of PIV images is drastically lowered because of the weaker Mie scattering intensity due to their smaller scattering cross-sectional areas [2]; (3) a stronger illumination may cure the problem associated with (2), but this can result in unwanted radiative heating of working fluid in the thermally driven flow measurements; and (4) the wall-reflection of the illuminated laser light seriously blurs PIV images particularly near the solid surfaces and the meniscus surface.

A microscopic PIV system using 200-nm fluorescent seeding particles successfully demonstrated its use microfluidics measurements although the technique suffered somewhat from the reduced spatial resolution associated with the statistical requirement for the necessary PIV image pairs [3]. For thermally driven flow measurements, the relatively large 200-nm seeding particles tend to accumulate near the evaporative thin film and coagulate onto the solid surface because of the surface tension adhesion, thereby altering the heat and mass transport characteristics. For this reason, the use of seeding particles of the smallest allowable size is necessary to minimize the accumulation problem.

[*]Corresponding author: kkihrn@rnengr.tarnu.edu

NOMENCLATURE

d capillary gone diameter
g acceleration due to gravity
h capillary pumping potential
ρ working fluid density
σ surface tension

SUBSCRIPTS

c condenser
e evaporator

The use of fluorescence compound dye molecules as seeding particles tan significantly alleviate the problem associated with seeding particle sire (1). Since the fluorescence emiting signal is usually several orders of magnitude stronger than the Mie scattering of the same scatterer size, the use of fluorescence dye molecules can massive the problems associated with (2) and (3). The laser-induced fluorescence (LIF) technique: tan exclusively record the fluorescence images after filtering out the pumping light band and this mummers the blurring problem in (4).

The use of caged fluorescence compound [4], which has long been utilized by enzymologists and cell biologists, seems to fulfill all the above requirements for a velocity mapping technique of miuo-scale flows. The essential idea is m use photo-activatable (caged) fluorophores (PAFs) that are optically uncaged by ultraviolet (UV) fight and are tacked by triggering their fluorescence with a visible light band. The dye used for the present study is a Dextran-caged fluorescein molecular dye that is initially unable m fluoresce, however, once it is exposed to ultraviolet radiation, the caging chemical group of the compound is cleaved and the molecule regains its photo-affinity to fluoresce. This uncaged fluorescence is activated upon exposure m a pumping band, usually in the visible range. The temporal migration of there uncaged fluorescence compounds allows for the determination of a velocity vector field. The engineering application of a similar idea was first introduced for flow visualization of bench-scale flow, fields [5] and the technique was later applied to measure the electroosmotic flow field developed in a microfluidic chancel [6]. The purpose of the present study is to apply the LIF-based velocimetry technique for feature research in the thermally driven flow field within a thin menixcus under heat

There has been a surge of interest in contact line heat transfer (Fig. 1) in recent years due to the recognition that the physics of the evaporating thin film is vitally important to the understanding of a wide range of two-phase heat transfer, applications including boiling, condensation, capillary pumped loops (CPL), micro heat pipes, and solidification with free surfaces. For, the CPL shown schematically in Fig. 1, the capillary pumping potential h is established by the differential of pore diameters, between the evaporator (e) and condser (c), and this potential drives the fluid circulation without an active flow circulation. For the molecular region, the evaporation is negligible due to the inherently small amount of mass involved. In the bulk pore region, the evaporation rare is also low since the surface temperature will not be sufficiently high because of the strong thermal resistance of the

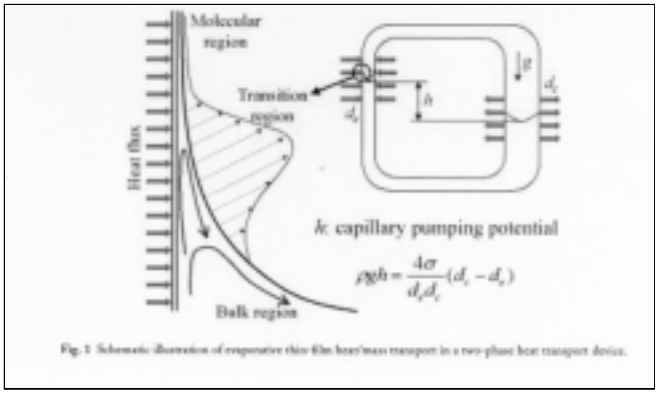

Fig. 1 Schematic illustration of evaporative thin-film heat/mass transport in a two-phase heat transport device.

bulk liquid. We predict analytically that the most heat and mass transport is taking place in the transition thin-film region of up to the order of 1 μm thickness [7].

Because of the inherently small scale of the evaporating thin film region, the microscopic heat and mass transport occurring in this region may hold the key to better understanding of the fundamental phenomena that have been examined largely using macroscopically observable phenomena. Although much progress has been made within the past few decades [8-10], complete understanding of the mechanisms has proved elusive primarily because of the lack of microscopic observable data. The flow field inside the evaporating meniscus and capillary pore is one of the missing observables, which can provide critical benchmarks against which the previously developed evaporative meniscus models can be evaluated.

The present study will briefly discuss the essential features of molecular tagging fluorescence velocimetry (MTFV) with an emphasis on its potential for micro-scale flow field mapping. We will also discuss the digitized analysis of fluorescence images to generate quantitative velocity vector fields. The technique has been applied to visualize the threedimensional flow occurring inside a heated capillary pore of 5-mm inside diameter (ID) with 5° inclination angle. Our results will show the meso-scale flow field data for the capillary pore bulk region and the beginning of the transition thin-film region.

EXPERIMENTAL SETUP

Figure 2 illustrates a schematic of the basic experimental setup for MTFV, which intrinsically resembles the fluorescence microscopy that was developed the early part of the 20th century, except that a monochromatic laser has substituted the bandpass-filtered light

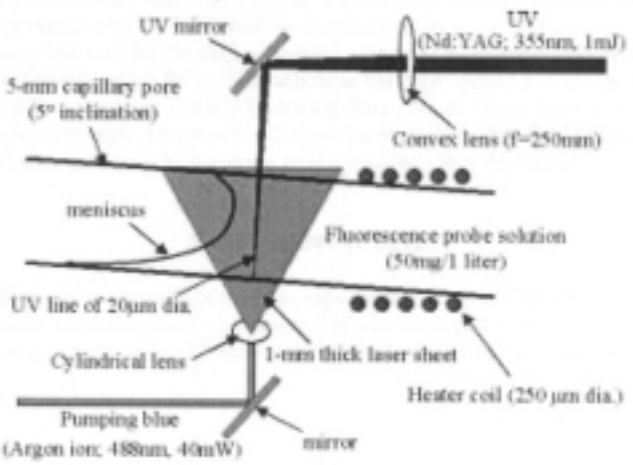

Fig. 2 Schematic illustration of molecular tagging fluorescence velocimetry (MTFV) system.

source. A triple harmonic ultraviolet neodymium:yttrium-aluminum-garnet (Nd:YAG) laser pulse of 8 mm diameter (λ=355 and adjustable from 100μJ to l0mJ) illuminates the rest field with a pulse duration of 5 to 6 ns. A density filter reduces the beam power to avid damage to the optical elements and an aperture reduces the beam diameter down to 5 mm to eliminate noise and diffused light from the edge of the beam. An ultraviolet convex lens with a focal length of 100 mm focuses the 5-mm diameter laser beam m a 20 μm diameter at the rest section. The rest section is a capillary pore mounted on a threedegree-of-freedom positioning system that is also 360 ° rotational. A 1-mm diameter continuous-wave (CW) argon-ion blue laser beam (λ=488 tam at 40 mW) illuminates the capillary pore test section from the opposite side of the ultraviolet (UV) laser. The blue beam is additionally filtered by a narrow bandpass interference filter to remove extraneous wavelengths of light incidentally produced by the argon-ion laser that can detrimentally induce uncaging of the caged Fluorescent dye. A cylindrical lens creates a thin blue laser sheet to illuminate uncaged fluorescence dyes in the rest section. The UV beam and thin blue sheet vertically pass through the symmetrical center plane of the capillary pore.

Tire rest section consists of a fused-silica capillary pore of 7-mm outside diameter (OD) and 5-mm ID, and the outer wall of the pore a wrapped with a nickel-chromium hearer wire of 250 μm diameter. The 5° tilted capillary pore establishes an 8-mm-long concave meniscus from the visible tip to the most receded bottom. The hearer wire a located 8mm above in the vapor region from the meniscus bottom, equivalently at the location of the tip of the meniscus, or 8 mm below the meniscus bottom in the liquid region.

The fluorescent dye used for the experiment was a dextran, DMNB-caged anionic fluorescein molecular dye with a molecular weight of 10,000g/mol which was manufactured by Molecular Probe, Inc, The absorption (pumping) maximum of the dye occurs at

494 nm, and the emission (fluorescence) maximum occurs at 518 nm. The probe is water-soluble and is mixed to a concentration of 50 mg/L of distilled, deionized water. This concentration is sufficient to induce images that are bright enough to be easily seen by the naked eye and captured by the CCD camera in the totally dark environment. While Lempert et al. [5] used a concentration ranging between 1 and 5 mg/L for their laboratory scale water tunnel experiment, this concentration proved to be far too low for smaller-scale experiments. Our experiment used a low-intensity UV beam to make a very thin line (d~20 μm) with minimal thermal effect, and a higher dye concentration was necessary. Also, Paul et al. [6] recommended a probe concentration of 5 mg dissolved in 3 mL of 0.1M sodium carbonate buffer with a pH 9.0. The dextran conjugates used for the presentexperiment are easily dissolved in water and the recommended concentration turns out to be a bit too high according to the criteria of Paul et al. [6]. Note that the optimum probe concentration depends on many local laboratory conditions including the pumping light intensity, test section dimensions, optical window characteristics, flow convection and diffusion, and sensitivity of recording means.

The fluorescence rise time for the uncaging evolution was estimated as short as 1 ms, that is, the fluorescence intensity quickly reaches a substantial level of the saturated intensity after the probe is short-pulsed by an UV beam. The evolution thereafter is a rather slow process that takes up to 0.5s until all the probes are fully uncaged or saturated [5]. The degree of uncaging achieved during the first quick rise within 1ms or so is sufficient to produce conceivable fluorescence images. Therefore, the temporal uncertainty due to the rise time on the order of 1 ms should be limited to an order of 0.1% of the true velocity tracking. The emission delay of the fluorescence after pumping is negligible in the nanosecond range and the spontaneous radiative lifetime of fluorescence in water is approximately 5 ns [1l].

The caging compound is inherently unstable and its instability is increased with exposure to high temperatures and ultraviolet light sources, including ambient light. The probe should be handled in a dark environment and stored at temperatures around -20 °C in the original powder and at around -4 °C in the water solution state to minimize spontaneous uncaging. The heating of the test fluid to induce the thermal flow may cause a degree of uncaging of the probe, which creates vaguely fluorescent background images. The actual fluorescence images of the UV uncaged probe is substantially brighter than the illusive background, which has been digitally subtracted from the recorded images. The fluorescence images are filtered out with a long-pass filter making 50% transmittance at 530nm to eliminate the pumping band as much as possible, and the filtered images are captured by a CCD video camera at a nominal 10 Frames per second (Fps).

RESULTS AND DISCUSSION

Both quantitative and qualitative visualization results are presented for the thin-film regions of heated capillary pore. All the presented results are for a 5-mm ID pore with 5 ° inclination from the horizon and for the fixed heater power at 3.0 W as a representative case. The flow patterns were similar up to about 10 W, beyond which boiling bubbles were generated and the meniscus became unstable.

Figure 3 shows sequential images of thermal bulk flows recorded at the vertical center plane of the capillary pore. The heater coil is located in the vapor region to the left

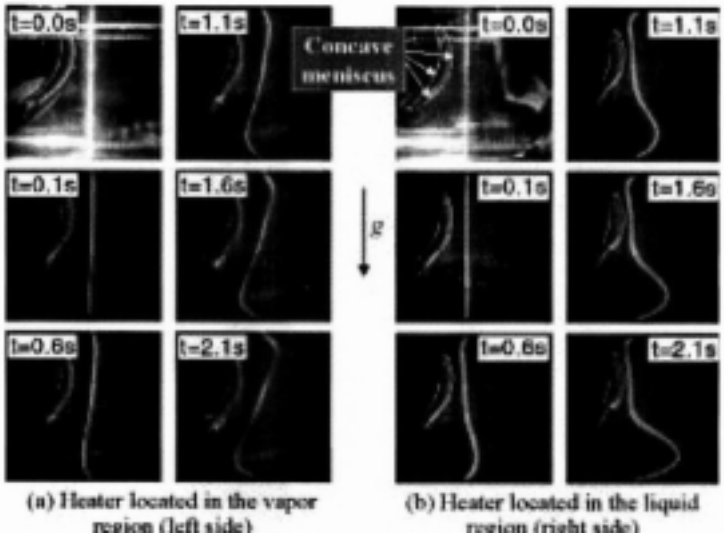

Fig. 3 Evolution of capillary bulk flows depending on the hearer locations.

of the meniscus in Fig. *3a,* and in the bulk liquid region to the right of the meniscus in Fig. *3b.* The first frames are taken at t= 0 when the UV uncaging pulse is applied and the initial thin line of the uncaged dye molecules is shown with the intense reflection of the UV from the pore inside glass surface. The subsequent frames represent the evolution of the uncaged dye as dictated by convection and diffusion. An interesting observation is that the lower part of the bulk flow is moving toward the heater location, on the symmetry plane, while the upper bulk flow is moving away from the heater for both cases of heater locations. These flow directions remain persistent to the thin-film region as shown in Figs. 4*a* and *b.* Note that the inverted and deformed upper portion of each image in Fig. 4 indicates the internally reflected and reduced image from the three-dimensionally concave meniscus surface. A colored version of Figs. 3 and 4 has been published as a photo gallery in the *journal* of *Heat Transfer* [12].

Figures 5 and 6 show velocity vector fields determined from the sequential images and their time interval of 1.0 s. The velocity fields calculated for the bulk flow (Fig. 5) are based on an assumption of stratified flows. This assumption may be questionable as the overall flow turns out to be fully three-dimensional and complicated, particularly for the flow near the meniscus surface and inside the thin film. Nevertheless, the bulk flow away from the meniscus shows largely stratified flow motions and the calculated velocity field should be a good approximation. For the wedge flows near the thin-film entrance (Fig. 6), the image displacement is calculated with a prorated slope assigned for each velocity vector location. This approximation is based on the fact that the thin-film flow is nearly parallel to the solid wall surface and is little affected by the curved surface. The flow vectors measured at the lower symmetry plane of the capillary are persistently directed toward the heater.

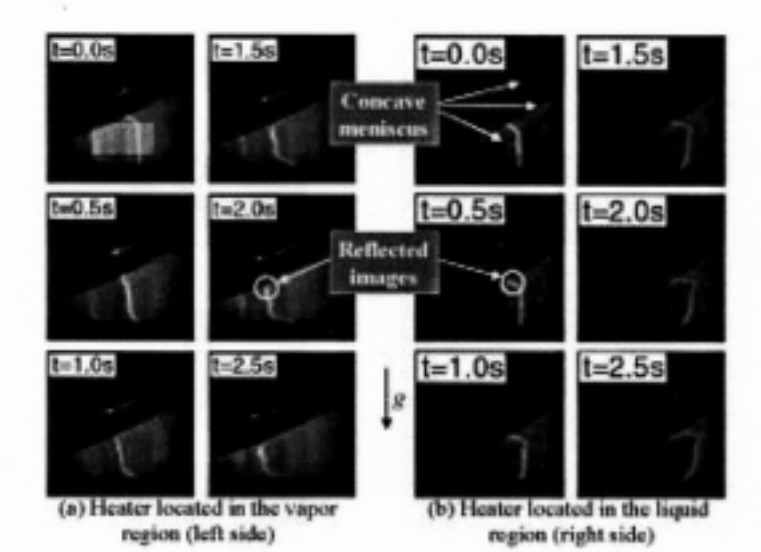

Fig. 4 Evolution of thin-film entrance region flows depending on the heater locations.

A principle that drives a surface flow pattern can be considered in the presence of temperature gradient. The surface tension coefficients of most liquids decrease with increasing temperature, and the surface tension gradient is called a thermocapillary stress, which slopes opposite to the temperature gradient. The thermocapillary stress drives the thermal flow parallel to the positive surface tension gradient, that is, to a cooler region since the cooler fluid of higher surface tension tends to draw the warmer fluid of lower surface tension. A good

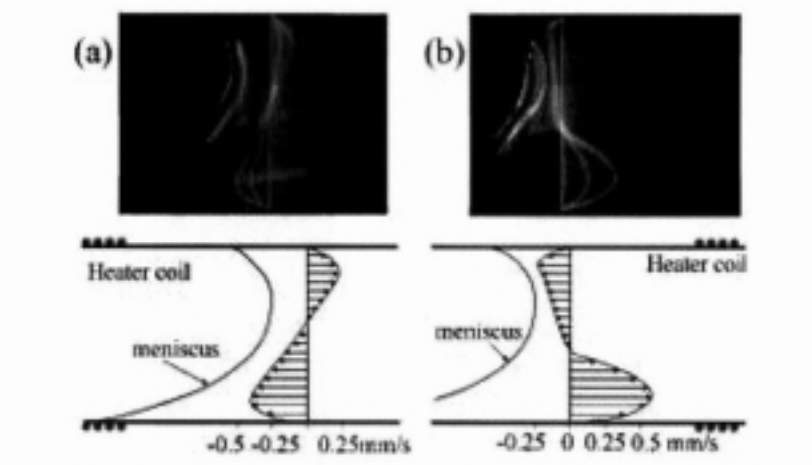

Fig. 5 Velocity vector fields for the bulk region calculated from the evolving fluorescence images.

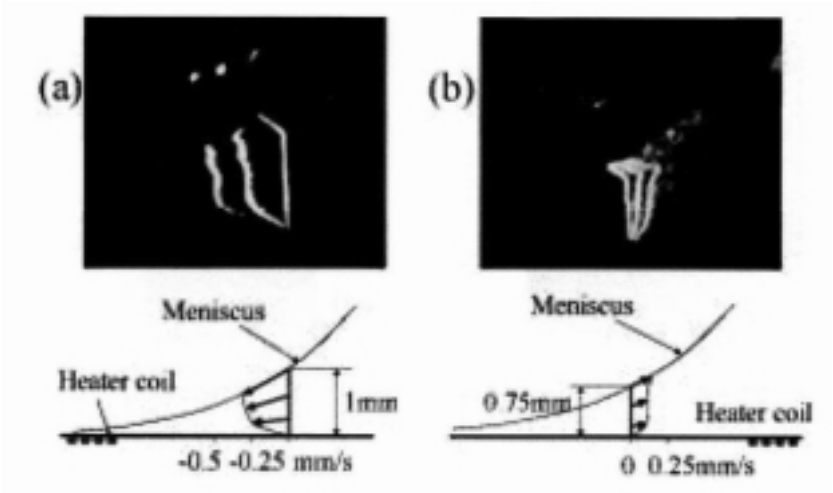

Fig. 6 Velocity vector fields for the thin-film entrance region calculated from the evolving fluorescence images.

example can be seen when a lighted match is suddenly dipped into a bowl of water and the radially outgoing surface flow is immediately driven by the surrounding cooler fluid.

This thermocapillary driving force exists inside a heated capillary pore and indeed critically contributes to determining the flow pattern inside. This effect increases in proportion to the temperature differential along the meniscus surface for a given fluid [13]. The flow fields mapped at the symmetry plane (Figs. 3-6), however, are not completely explained by the thermocapillary phoretic effect alone since the observed flows are driven toward the warmer side near the heater, which apparently conflicts with the thermocapillary phoretic nature. As will be shown below, the reason for the apparently opposite flow directions is explained by the three-dimensional nature of the whole flow and additional convective buoyancy drive for the pore region. The MTFV measurement planes have been extended and rotated to cover the fully three-dimensional flows, including the detailed surface flow motion on the meniscus as well as the bulk flow in the pore. These extended measurements could not be used to calculate vector profiles of the whole three-dimensional region because the fluorescence line did not stay in the laser sheet plane and the dye molecules were diffused too quickly by the strong flow circulation.

Figures 7 and 8 show the qualitative flow patterns obtained from the extended visualization. The flows are fairly symmetrical with respect to the vertical center plane thus, only one-half of the capillary pore domain is presented. The distance from the meniscus front (*A*) to the deepest concave point on the meniscus is measured to be approximately 8mm. For the heater installed in the vapor region (Fig. 7), the hottest spot on the meniscus surface is located at the closest leading edge of the meniscus (*A*) and the coldest spot on the meniscus surface is at the opposite point *(B)* on the same symmetry plane. The thermocapillary stress between the two spots drives the heated fluid flow on the meniscus surface along the pore inner curved wall from *A* to *B* on the meniscus surface. Once the flow reaches *B,* partial flow is driven through the top half of the pore to the bulk region *C* as a result of the natural convection in the pore. The remaining flow from *B* returns to *A* along the centerline and this returning flow induces the bulk flow from the lower half of the pore toward *D* and then to *A*.

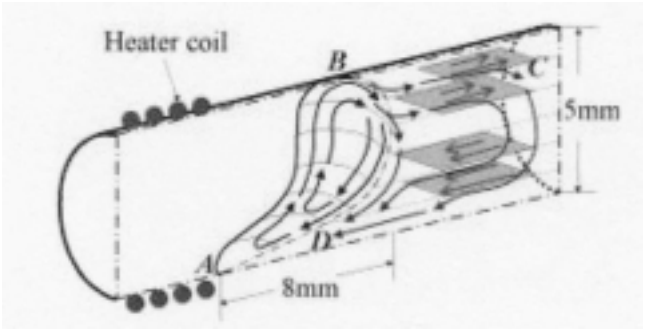

Fig. 7 Three-dimensional flow estabilishment in a nearly horizontal capillary pore heated in the vapor region.

The heavier cooled liquid descends from *C* to the lower region and joins with the induced flow at *D*. This induced flow constitutes the mass continuity by compensating for the splitting flow near the top *B* and for the evaporative flux on the meniscus surface. The overall capillary pore flow is made up of a combined thermocapillary-driven meniscus surface flow with the induced bulk flow. The convective circulation heating is completed as the two flow regimes compensate each other satisfying the mess continuity.

When the hearer is installed in the liquid region (Fig. 8), all of the flow directions and rotations are reversed. *A'* and *B*' represent the hottest and coolest spots on the meniscus surface, respectively, *C*' denotes the bulk region where the partial flow from *B'* is driven to, and *D'* denotes the region whey the induced flow from the bulk merges into the surface near *A'*. Again, the thermocapillary action doves the meniscus surface flow gum *A'* to *B'* along the capillary inner m,,dI waft and the Bow returns along the center of the meniscus surface. The heater mil a located 8 mm away from the deepest meniscus point to beat the liquid region by direct natural convection (whereas the hearer located in the vapor region for the ruse of Fig. 7 heats the vapor and the meniscus tip region to induce a convective hearing for the bulk flow). Note that the stronger corrective flow

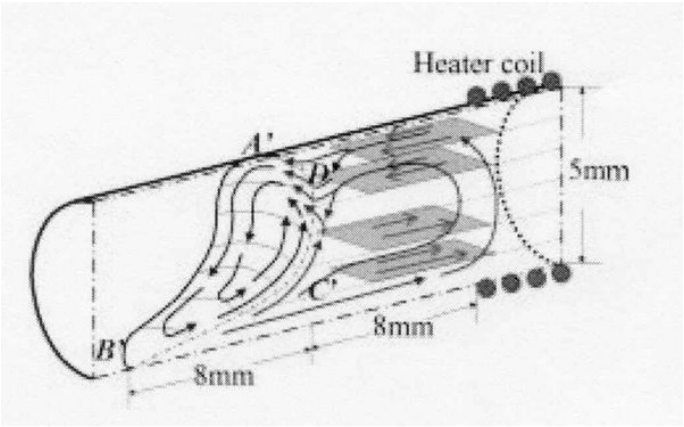

Fig. 8 Three-dimensional flow establishment in a nearly horizontal capillary pore heated in the liquid region.

driven by the heater coil meets the induced ascending stream from *C*' and the resulting bifurcated flows merge into the surface flow near *D*'.

The natural convection directly imposed on the liquid region drives a stronger natural convection circulation in the bulk region. The buoyant rise of the heated liquid inevitably draws the flow from *B*' to *C*', and the flow returns to the surface region *D*' and *A*' to compensate for the induced flow to the bulk at *C*' and for the surface evaporation. The overall capillary flow for the liquid heating consists of the thermocapillary driven meniscus surface flow and convective buoyancy driven bulk flow, instead of the induced bulk flow shown for the previous case of the vapor heating. The convective driven bulk flow should be relatively faster than the induced bulk flow and this is evidenced in the previous quantitative velocity comparison showing the former being faster than the latter for the same amount of the heat flux (Figs. 5 and 6). For the case of meniscus surface flow, however, the vapor heating case shows faster flow than the liquid heating case since the former generates larger temperature gradients along the surface.

CONCLUSIONS

We have developed a molecular tagging fluorescence velocimetry (MTFV) system for use in meso- to micro-scale thermally driven flow mappings. In this paper we present preliminary results for meso-scale three-dimensional thermal flows inside a heated 5-mm capillary pore. The visualization results show that the thermocapillary stress plays a critical role in determining the meniscus surface flow characteristics while either an induced convection or a direct convection heating drives the bulk region flow behaviors. Accordingly, the vapor heating generates faster thermocapillary-driven surface flows while the liquid heating results in faster convection-driven bulk flows. The exclusive use of nanosized dye molecules along with the MTFV technique carries strong potential as a diagnostic means to measure micro-scale flow field mapping.

REFERENCES

1. M. Raffel, C. Willett, and J. Kompenhans, *Particle Image Velocimetry,* Springer, 1998.
2. Van de Hurst, *Light Scattering by Small Particles,* Dover, 1957.
3. C. D. Meinhart, S. T. Wereley, and J. G. Santiago, PIV Measurements of a Microchannel Flow, *Experiments in Fluids,* vol. 27, pp. 14-419,1999.
4. G. Martin, *Metbods in Enzymology, vol. 291 Caged Compounds,* Academic Press, San Diego, CA, 1998.
5. W. R. Lempert, K. Magee, P. Ronney, K. R Gee, and R P. Haugland, Flow Tagging Velocimetry in Incompressible Flow Using Photo-Activated Nonintrusive Tracking of Molecular Motion (PHANTOMN), *Experiments in Fluids,* vol.18, pp. 249-257,1995.
6. P. H. Paul, M. G. Garguilo, and D. J. Rakestraw, Imaging of Pressure and Electrokinetically Driven Flows through Open Capillaries, *Anal. Cbem., vol.* 70, pp. 2459-2467,1998.
7. S. Moosman, and G. M. Homsey, Evaporating Menisci of Wetting Fluids, j. *Colloid Interface* Sci., vol. 73, No. 1, pp. 212-223,1980.
8. F. J. Renk, and P. C. Wayner, An Evaporating Ethanol Meniscus, *ASME J. . Heat Transfer,* vol.101, pp. 55-58 (Part I) and pp. 59-62 (Part II), 1979.

9. P. C. Wayner, C. Y. Tung, M. Tirumala, and J. H. Yang, Experimental Study of Evaporation in the Contact Line Region of a Thin Film of Hexane, *ASME J. Heat Transfer,* vol.107, pp. 182-189, 1985.
10. R Reyes, and P. C. Wayner, A Kelvin-Clapeyron Adsorption Model for Spreading on a Heated Plate, *ASME J. Heat Transfer, vol.* 118, pp. 822-830,1996.
11. R F. Chen, G. G. Burek, and N. Alexander, Fluorescence Decay Times: Proteins, Coenzymes, and Other Compounds in Water, *Nature,* vol.156, pp. 949-951,1967.
12. J. S. Park, K. D. Kihm, and D. M. Pratt, Lagrangian Flow Mapping of Heated Capillary Pore and Thin Film Using Molecular Fluorescence Velocimetry (MFV), *ASME J Heat Transfer,* vol.122, 2000.
13. D. M. Pratt, J. R Brown, and K Hallinan, Thermocapillary Effects on the Stability of a Heated, Curved Meniscus, *ASME J. Heat Transfer, vol.* 120, 1998.